Magnesium Technology 2013
Edited by: Norbert Hort, Suveen N. Mathaudhu, Neale R. Neelameggham, and Martyn Alderman
TMS (The Minerals, Metals & Materials Society), 2013

Magnesium Technology 2013

Creep

Magnesium Technology 2013
Edited by: Norbert Hort, Suveen N. Mathaudhu, Neale R. Neelameggham, and Martyn Alderman
TMS (The Minerals, Metals & Materials Society), 2013

COMPRESSIVE CREEP PROPERTIES OF WROUGHT HIGH TEMPERATURE MAGNESIUM ALLOYS IN AXIAL AND TRANSVERSE ORIENTATION – A NEUTRON DIFFRACTION STUDY

D. Sediako[1] , L. Bichler[2], M. van Hanegem[2] and S. Shook[3]
[1]Canadian Neutron Beam Centre, Chalk River, Canada
[2]University of British Columbia – Okanagan, School of Engineering, Kelowna, Canada
[3] TH Magnesium Inc., Farmington Hills, MI, USA

Keywords: Magnesium alloys, high-temperature creep, neutron diffraction

Abstract

Magnesium alloys developed for high temperature applications may become a material of choice in structural components exposed to elevated temperatures, for example, around automotive front end structures. Performance of wrought materials, however, often depends on the direction of the load with respect to the extrusion direction.

This study focused on investigating compressive creep response of three extruded magnesium alloys: AE42, EZ33 and ZE10 in the longitudinal and transverse directions. In-situ neutron diffraction experiments on evolution of primary and secondary creep strain at 175°C, 50MPa load for the duration of 24 hours was studied for several crystallographic planes.

The results suggest that the AE42 alloy exhibited significant strain fluctuations on the basal (0002) and $(10\bar{1}2)$ planes, possibly related to plastic deformation processes of grain boundary sliding or twinning. In contrast, EZ33 and ZE10 alloys had a significantly lower and more uniform strain deformation in both elastic and plastic regime. Microstructure analysis revealed that the AE42 alloy consisted of large $Al_{11}RE_3$ particles with $Mg_{17}Al_{12}$ phase forming around Al-RE particles and in intergranular regions, while the aluminum-free alloys contained complex intermetallics on the grain boundaries, as well as Zn-RE nanoscale dispersoids throughout the matrix.

Introduction

The primary challenge with utilizing more Mg alloys in vehicles stems mainly from their relatively high cost (~50% higher than that of aluminum alloys) and their poor creep resistance above 120 °C. The loss of strength at elevated temperatures has been attributed to grain boundary movement and plastic deformation, which ultimately lead to inter-granular failure [1]. Enhancing the creep resistance of magnesium alloys has therefore been the subject of intense international research efforts.

Magnesium with its HCP crystal structure is known to have only a limited number of slip systems. In general, slip most readily takes place on the close-packed basal plane (0002) followed by a secondary slip on the $(10\bar{1}1)$ planes [1]. The addition of rare earth elements (REs) to aluminum containing magnesium alloys was seen to significantly increase creep resistance due to the formation of thermally stable intermetallic compounds along the grain boundaries [2]. The low solubility of REs in Mg results in the formation of $(Mg,Al)_xRE_y$ complex intermetallics, which decreases the Al saturation in the matrix and decrease the possibility of undesirable β-phase formation [3].

The addition of REs to Mg-Zn alloys has been also seen to increase creep resistance due to precipitation hardening [4]. Mg_xRE_y and Mg_xZn_y intermetallic compounds readily form in EZ magnesium alloys due to the low solid solubility of REs in Mg. Additional RE_xZn_y intermetallic compounds on the grain boundaries were seen to remain stable at temperatures as high as 420°C [5]. With the increasing concentration of rare earths, presence of fine precipitates dispersed throughout the matrix was reported. The role of these precipitates, however, on the creep performance required further study [6].

In this research, the longitudinal and transverse compressive creep strain of AE42, EZ33 and ZE10 wrought alloys was measured using an *in-situ* neutron diffraction technique. The creep performance was subsequently related to the alloy microstructure and the observed creep strain anisotropy is discussed.

Experimental Setup

Alloy samples were produced by Timminco Corporation Canada via proprietary controlled-cooling permanent mold casting followed by hot extrusion. Quality of all cast and extruded samples was inspected with respect to inclusions, cracking and porosity. The composition of the alloys conformed to the ASTM composition limits for each alloy.

The extruded alloys were machined to cylindrical specimens according to the ASTM E139-70 standard for compressive creep testing of Mg alloys. The longitudinal axis of the cylindrical test specimen was aligned either with the extrusion axis (EA) of the billet, i.e., along the longitudinal (L) direction parallel to EA or along the transverse (T) direction perpendicular to EA. Compressive creep strain and microstructure were studied in these two directions.

Neutron Diffraction

Compressive creep strain *in-situ* measurements were carried out at the National Research Council-Canadian Neutron Beam Center (NRC-CNBC) in Chalk River, ON. Material samples were maintained at 175°C with infrared heaters, and then loaded in compression at 50MPa over a 24 hour period. Elastic creep microstrain was measured using the peak-shift method for the $(10\bar{1}0)$, (0002), $(10\bar{1}1)$, $(10\bar{1}2)$ and the $(2\bar{1}\bar{1}0)$ planes. In addition to measuring crystallographic strain, a traditional extensometer was used to measure the total (plastic and elastic) compressive creep strain during the experiment. A detailed description of the neutron diffraction experiments, set-up and methods of calculating compressive strain has been published by the authors earlier [7].

Optical and Electron Microscopy

Alloy samples were prepared for microstructure analysis using standard polishing procedures for Mg alloys. AE42 alloy was etched with acetic glycol to reveal the grain size and general microstructure. EZ33 and ZE10 alloys were etched using dilute nitric acid to reveal second phases. Optical microscope (Zeiss AxioObserver) and scanning electron microscope (Tescan Mira-3) with XEDS capability were used to study the alloy microstructure and chemical composition.

Results and Discussion

Neutron Diffraction Creep Microstrain Measurement

The results of compressive creep measurements using an extensometer are provided in Figure 1. The values show the combined plastic and elastic creep strain during the test. In both orientations (L and T), the AE42 alloy experienced the greatest compressive creep, while EZ33 and ZE10 alloys showed an order of magnitude smaller strain. Further, the results suggest that the AE42 alloy continued to creep with time, while the EZ33 and ZE10 alloys reached a stable creep strain after a short primary creep stage, and remained at this creep level for the remainder of the test. Consequently, the results suggest that aluminum-free alloys were significantly more stable than current industry high-temperature benchmark AE42 alloy.

The duration of the creep test ranged from 12 – 24 hours for the samples tested in the L direction, and from 23 - 100 hours for the samples tested in T direction. By extrapolating the data points of the secondary creep stage (linear portion with constant slope on the creep curve in Figure 1) the creep strain at 100 hrs was estimated for all the samples. In the case of the AE42 alloy, the creep strain in the transverse direction was ~38% greater than in the longitudinal direction, with a total alloy average strain of 11.8% after 100 hrs. In contrast, at 100 hrs, both EZ33 and ZE10 alloys outperformed the AE42 alloy in creep resistance, with an average creep strain of only 0.07% and 0.17%, respectively, as seen in Figure 2a.

Figure 2b summarizes the relative creep resistance of each alloy based on the ratio of creep strain in the L- and T-directions. The results indicate that the AE42 and ZE10 alloys exhibited comparable strain isotropy in both directions, while the EZ33 alloy deformed readily in the transverse direction (0.12%), but exhibited good creep resistance in the longitudinal direction (0.03%). Thus, the response of the EZ33 alloy was highly anisotropic. This result will be related to the alloy's microstructure, as will discussed in subsequent sections.

The results of *in-situ* elastic creep strain measurement via neutron diffraction are presented in Figure 3 (Longitudinal direction) and Figure 4 (Transverse direction). The data presented in Figures 3 and 4 indicates that all the samples generally come to the steady state creep (secondary creep) within the first two hours of loading. Following this, the elastic microstrains obtained in the neutron diffraction experiments remain relatively constant. This validates the strain-extrapolation approach adopted in this study to estimate the 100-hr strains presented in Figure 2.

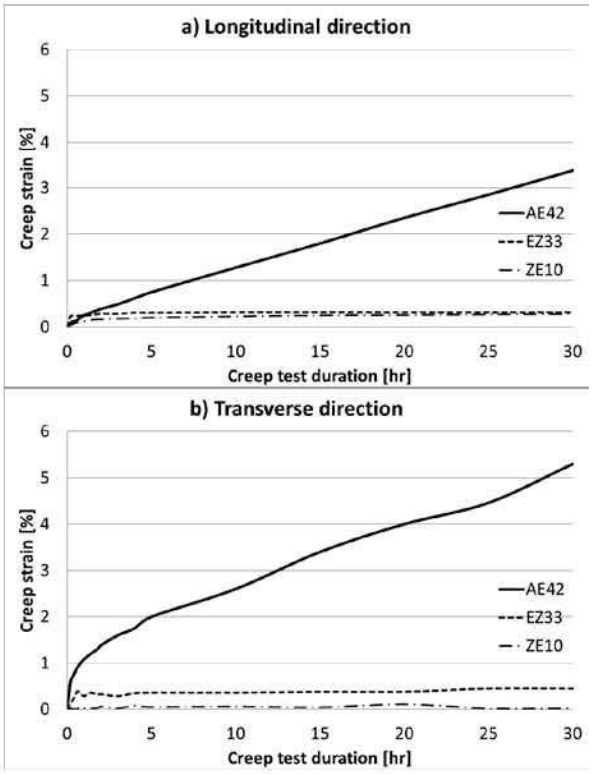

Figure 1: Compressive total (plastic + elastic) creep strain in: a) Longitudinal direction, and b) Transverse direction

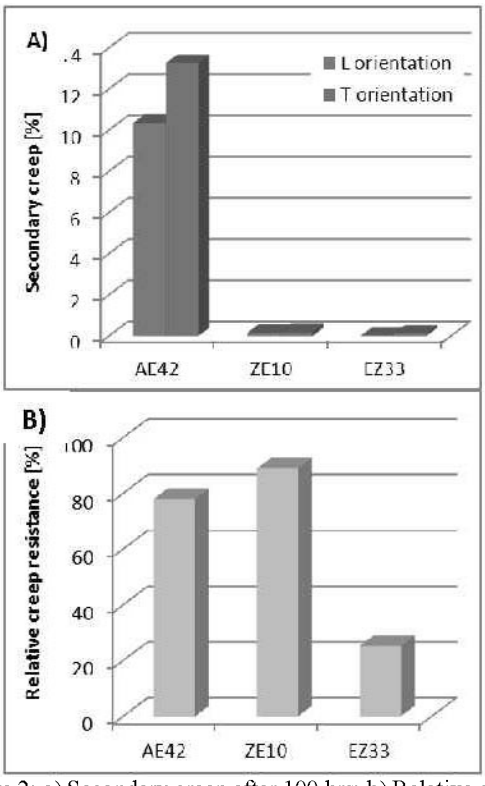

Figure 2: a) Secondary creep after 100 hrs; b) Relative creep anisotropy ($\varepsilon_{trans}/\varepsilon_{long}$)

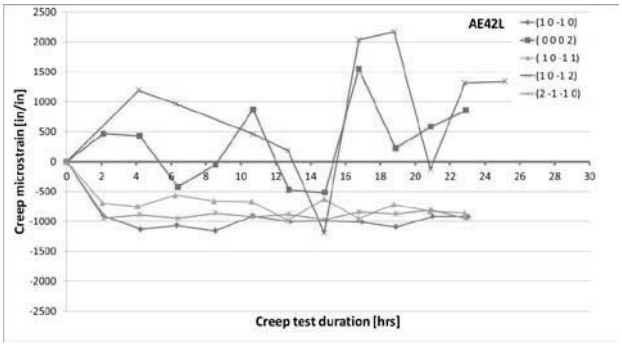

a) AE42 alloy

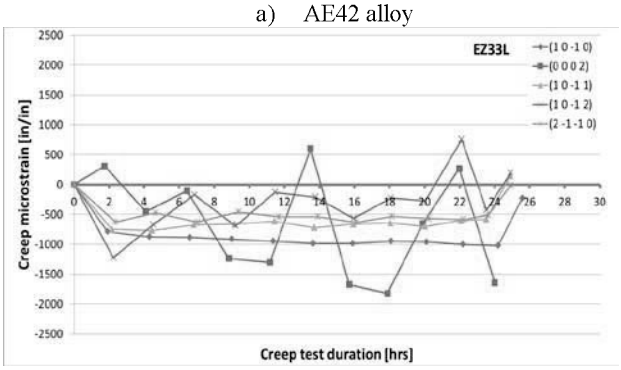

b) EZ33 alloy

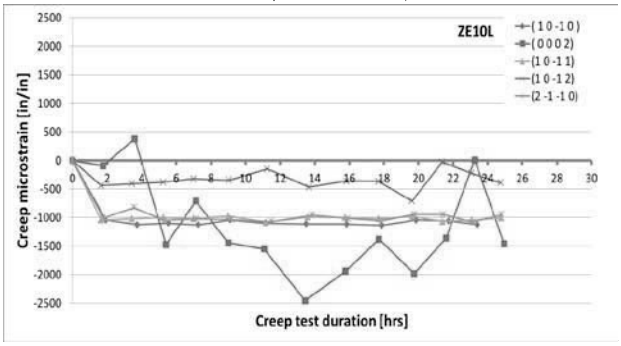

c) ZE10 alloy

Figure 3: Creep microstrain in the longitudinal direction.

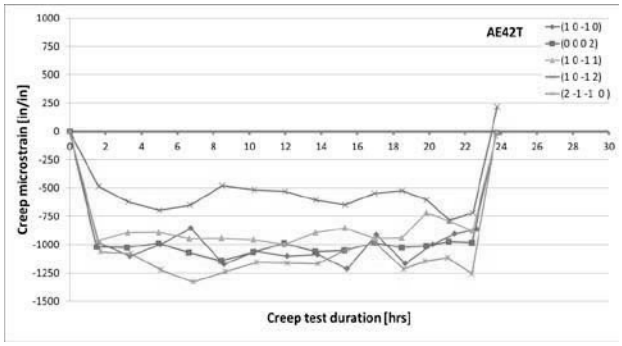

a) AE42 alloy

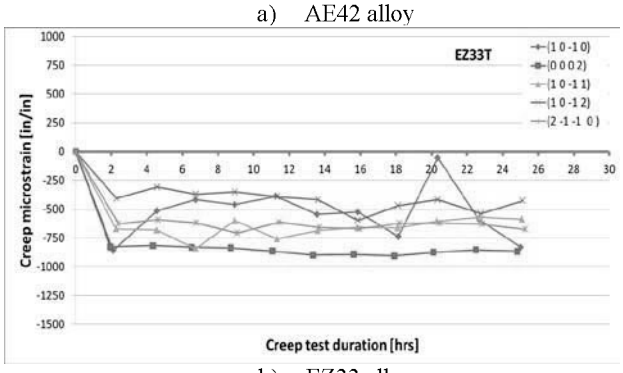

b) EZ33 alloy

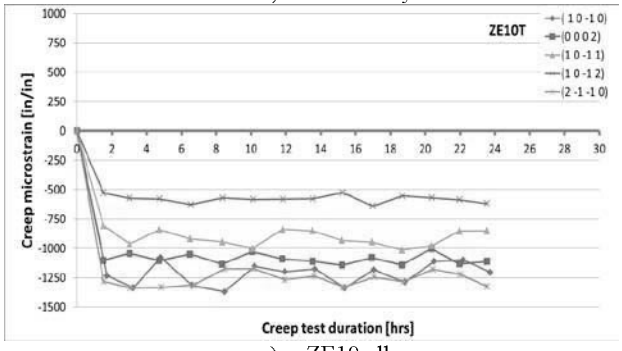

c) ZE10 alloy

Figure 4: Creep microstrain in the transverse direction

Longitudinal Direction

It was observed that the creep strain on the close packed basal plane (0002) in all alloys exhibited the greatest fluctuations during the creep test. This result was related to the strong basal texture frequently observed in the extruded samples, with a very high tendency of the (0002) poles to align perpendicular to the EA. The texture may get further modified as a result of creep-induced deformation [8]. Although the load on the cylindrical specimens remained compressive at all times during the test, the (0002) basal planes often exhibited tensile – compressive - tensile strain fluctuations, particularly in the case of the AE42 alloy. These fluctuations were likely an indicator of plastic deformation processes via grain reorientation (due to grain boundary sliding) and/or due to localized twinning. The authors have reported on twinning of the AE42 alloy during compressive creep earlier [9].

The presence of twinning was also suggested by observing the microstrain profile for the $(10\bar{1}2)$ plane, which is a preferred twin plane in Mg alloys, and was seen to exhibit significant strain reversal oscillations. The strain on the remaining crystallographic planes was seen to remain relatively uniform. In the case of the aluminum-free alloys EZ33 and ZE10, the creep microstrain remained uniform, with the exception of (0002) basal plane fluctuations. These fluctuations, however, remained predominantly in the compressive state, unlike in the AE42 alloy where tension evolved. It is of interest to note, that twinning was not observed in the EZ33 or ZE10 alloys, which is in agreement with the uniform strain on the $(10\bar{1}1)$ and $(10\bar{1}2)$ planes.

Transverse Direction

The elastic strain response of the studied crystallographic planes varied depending on the sample loading direction, as seen in Figure 4, a-c. The compression-tension (0002) strain fluctuations observed in the L-samples were not readily observed in the T-samples. It is suggested that as grain boundary sliding likely occurred parallel to the *c*-axis of the grains (due to the strong extrusion-type basal texture), the basal plane strain was less affected and remained relatively constant for the T-samples.

The magnitude of the (0002) microstrain in the AE42 alloy was ~1000 [in/in], which was of the same order of magnitude as the strain on the remaining crystal planes. The only exception was the microstrain on the $(10\bar{1}2)$ plane, which was less stable and reached only -700 [in/in]. Such relative decrease in elastic strain values frequently indicates reduced yield strength of the material, resulting in enhanced plastic deformation of the material [10]. The lower values of microstrain on $(10\bar{1}2)$ planes may therefore indicate higher levels of plastic deformation on these planes. It is likely that this plastic deformation, however, was not necessarily accommodated by twinning, since the level of microstrain remained relatively constant. Similar observation was made for the other alloys as well.

The range and magnitude of the microstrain recorded for the L-oriented samples are comparable to the values recorded for the T-oriented samples (see Table 1). The close proximity of the results for the AE42 and ZE10 suggests relative deformation isotropy for the two alloys in both orientations. In contrast, significant reduction of microstrain for the T-oriented sample of EZ33 alloy as compared to the values for L-oriented sample indicate anisotropy in plastic deformation of this alloy in the two orthogonal orientations, also observed in the analysis of the relative creep resistance of the alloys (Figure 2). This observation may have far-reaching practical implications, indicating limitation in the application of this alloy in the structural components subjected to elevated temperatures and directional load.

Table 1: Range of microstrain for $(10\bar{1}0)$, $(10\bar{1}1)$ and $(2\bar{1}\bar{1}0)$ crystallographic planes.

Alloy	Microstrain range for the L-oriented samples	Microstrain range for the T-oriented samples
AE42	-600 -1100	-800 -1250
EZ33	-500 -1000	-500 -700
ZE10	-1000 -1100	-800 -1350

Alloy Microstructure

Optical micrographs of the post-creep alloys are provided in Figure 5 and 6. The evident extrusion texture observed in the AE42 and EZ33 alloys reveals that second phases strongly segregated between the elongated grain boundaries in the longitudinal direction. In contrast, ZE10 alloy had intermetallics relatively uniformly dispersed throughout the microstructure in both directions.

The AE42 alloy contained massive Al-RE intermetallics (Black particles in Figure 5a and 6a), which exhibited severe fracturing as a result of creep testing, as seen in Figure 7. These phases consisted of Mg–(32 wt%Al, 27wt%Ce, 21 wt%La, 6wt% Nd) and traces of Pr, as determined from SEM-XEDS analysis. It has been established that La:Nd ratio below 0.7 promotes formation of Al_2RE phase, whereas higher La:Nd ratios promote formation of $Al_{11}RE_3$ phase [3]. Thus, these large acicular particles were likely the metastable $Al_{11}RE_3$ phase, which possibly began softening and degrading as a result of elevated temperature exposure. In addition, the metastable $Mg_{17}Al_{12}$ (β)-phase was also observed at the grain boundaries and in the vicinity of the $Al_{11}RE_3$ particles (medium gray in Figure 5a), possibly suggesting that exposure to the test conditions was sufficient to activate Al atom mobility. Consequently, the eutectic β-phase formed with its relatively low melting temperature and contributed to grain boundary sliding and reduced the effectiveness of grain boundary pining by the Al-RE complex intermetallics during creep. The grain interior of the AE42 alloy contained extensive lens-shape twins, as illustrated in Figure 8. Twinning was not observed in any of the aluminum-free alloys.

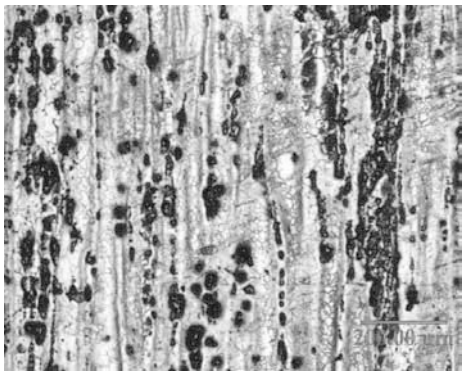

a) AE42

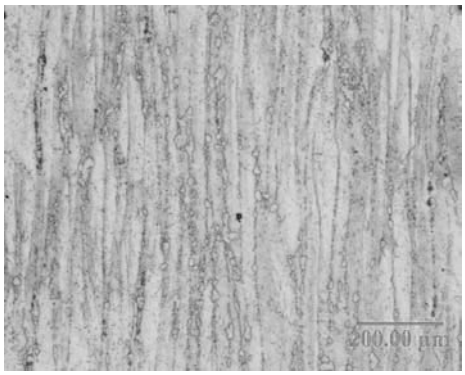

b) EZ33

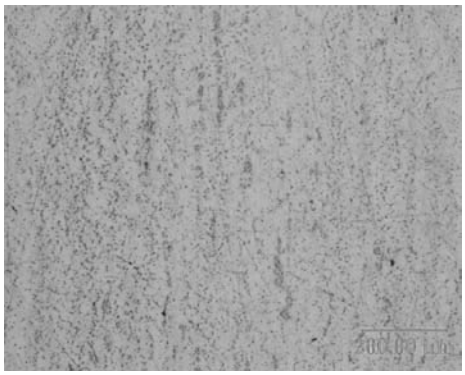

c) ZE10

Figure 5: Alloy microstructure in longitudinal direction

Similar to AE42, the EZ33 alloy had intermetallics agglomerated in the intergranular regions as well. However, the intermetallics were significantly smaller in size and more uniformly distributed, as seen in Figure 6b and 9. The EZ33 alloy contained three dominant types of intermetallic compounds, as seen in Figure 9: "A" – large gray particles consisting of Mg-(13wt%Zn, 11wt%La, 14wt%Ce, 2wt% Nd), "B" – fine white particles of Mg-(13wt%Zn, 6wt%La, 13wt%Ce, 3wt%Nd,7wt% Zr), and "C" – nanoscale dispersoids of Mg-(3wt%Zn, 0.9wt%Ce, 0.3wt%Nd).

As seen in Figure 9, the nanoscale particles were homogeneously dispersed throughout the microstructure in both directions. The precipitates "A" and "B" appeared to be present along most of visible grain boundaries in the longitudinal alloy samples.

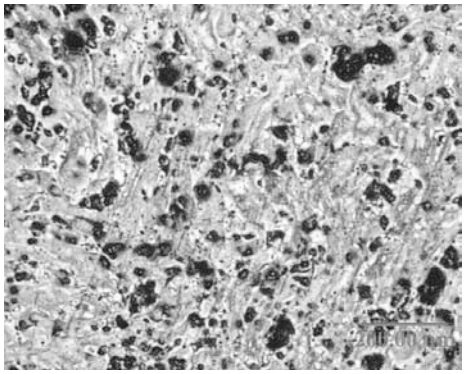

a) AE42

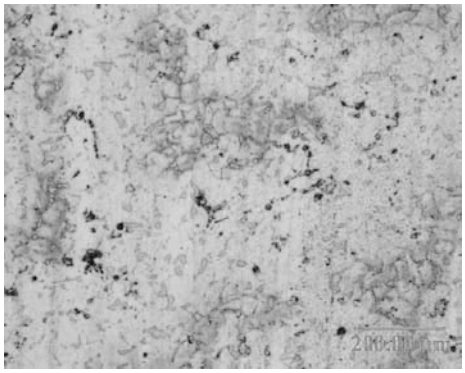

b) EZ33

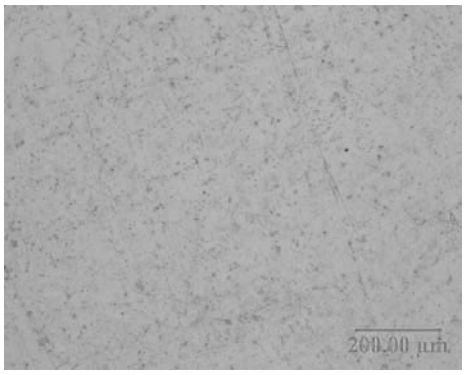

c) ZE10

Figure 6: Alloy microstructure in transverse direction

In contrast, these particles were not homogeneously distributed in the transverse direction, and only fractions of grain boundaries contained these intermetallics. This observation possibly supports the high strain anisotropy recorded in the EZ33 alloy with the extensometer (Figure 2b). In the longitudinal direction, grain boundary sliding was inhibited by the pinning effect of the precipitates, as also confirmed by the ND results in Figure 4 (elastic strain relaxation due to plastic deformation was more prominent in the transverse sample). In contrast, deformation in the transverse direction was relatively easier due to available grain boundaries where grain boundary pinning was not successfully achieved.

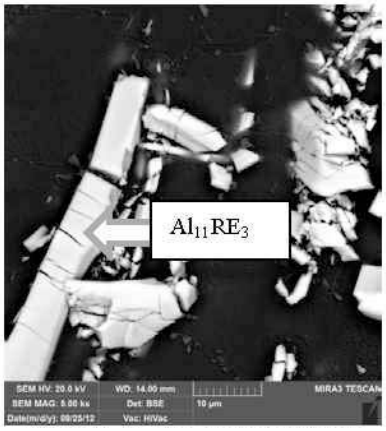

Figure 7: $Al_{11}RE_3$ phase fracturing

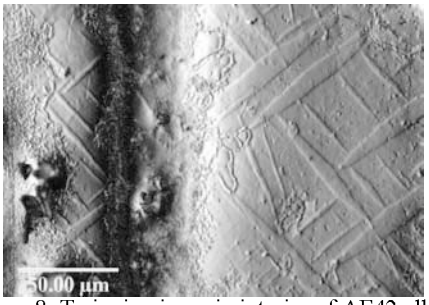

Figure 8: Twinning in grain interior of AE42 alloy

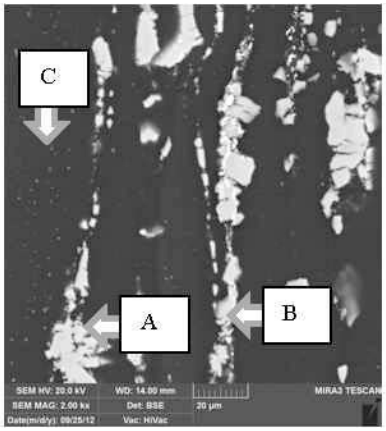

a) Longitudinal section

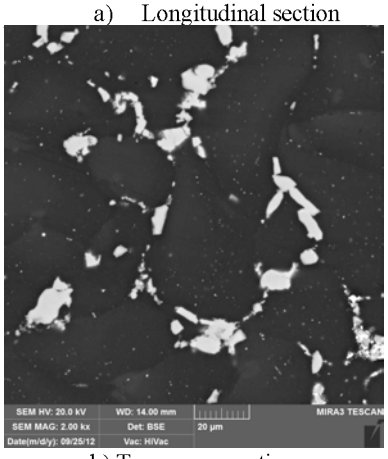

b) Transverse section

Figure 9: Microstructure of EZ33 alloy

The ZE10 alloy's microstructure appeared to be very homogeneous in both directions (L and T) as seen in Figure 5c and 6c. Complex intermetallic aggregates as seen in Figure 10 were identified via SEM/XEDS: "A" - dark gray particles with Mg-(8wt%Zn, 8wt%Zr, 7wt%La, 11wt%Ce, 2wt%Nd), "B" – fine white particles with Mg-(3wt%Zn, 36wt%Zr, 3wt%La, 4wt%Ce and 1wt%Nd) and "C" – nanoscale dispersiods with Mg-(3wt%Zn, 1wt%La, 2wt%Ce). The second phases appeared to be smaller and relatively uniformly distributed in both (L and T) directions. Consequently, the relatively uniform creep response (Figure 2b) in both directions was likely the result of homogeneous microstructure and dispersion strengthening by precipitates on the order of 0.5 – 2 μm in diameter. Presence of these very fine dispersoids (as in the EZ33 alloy) would significantly inhibit plastic flow within the grains or any twining. Observation of grain interiors in the EZ33 and ZE10 alloys did not reveal presence of twins.

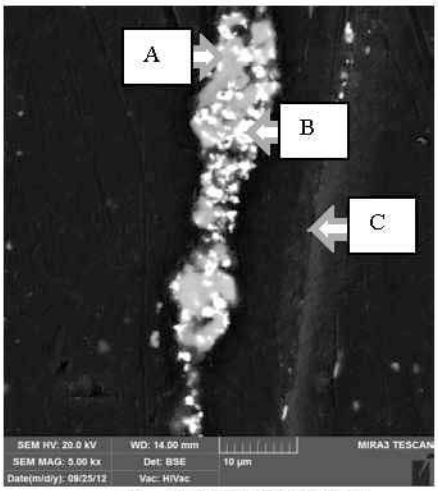

a) Longitudinal section

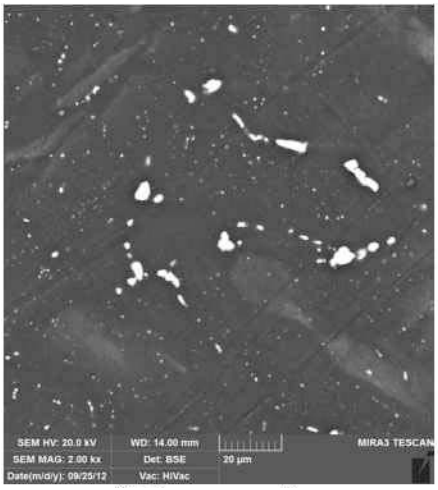

b) Transverse section

Figure 10: Microstructure of ZE10 alloy

Conclusions

The findings of this research demonstrate that neutron diffraction successfully enabled quantitative characterization of anisotropic creep strain in selected high-temperature magnesium alloys. The results suggest that:

1) The total compressive creep strain for the AE42 alloy was an order of magnitude greater than for EZ33 and ZE10 alloys tested at 175 ºC and 50 MPa.
2) The EZ33 alloy had a typical extrusion-type microstructure. Also, the microstrain response was highly anisotropic in the T- direction.
3) The ZE10 alloy, although extruded, had a relatively homogeneous microstructure, with fine second phases. Further, this alloy had uniformly dispersed Mg-Zn-RE nanoscale particles, which likely prevented twinning and plastic deformation during creep.

Acknowledgement

The authors acknowledge the financial support from the National Science and Engineering Research Council (NSERC) Discovery grant. We also thank the staff at NRC-Canadian Neutron Beam Center for their valuable assistance in performing neutron diffraction experiments.

References

1. Haughton, J.L. and Prytherch, W.E., *Magnesium and its alloys* (London, Dept. of Scientific and Industrial Research, 1937).
2. K. M. Asl, A. Tari, and F. Khomamizadeh, "The effect of different content of Al, RE and Si element on the microstructure, mechanical and creep properties of Mg-Al alloys", *Materials Science and Engineering,* (A 523) (2009), 1-6.
3. B. R. Powell *et al*. "Microstructure and creep behavior in AE42 Magnesium die-casting alloy", *J. of Metals*, 54(8) (2002), 34-38.
4. J. Yan et al, "Creep deformation mechanism of magnesium-based alloys", *J. of Material Science*, 43 (2008) 6952-6959.
5. T. Ryspaev et. al. "Microstructure of superplastic QE22 and EZ33 magnesium alloys", *Materials Letters*, 62 (2008) 4041-4043
6. T. Zhou, T., H. Xia, and Z.H. Chen "Effect of Ce on microstructures and mechanical properties of rapidly solidified Mg-Zn alloy" *Mat. Sci. and Technology*, 27(7) (2011) 1198-1205.
7. D. Sediako et al. "Application of neutron diffraction in characterization of texture evolution during high-temperature creep in magnesium alloys" Can. Nuclear Soc. Meeting 2010
8. M. Celikin et. al., " Compressive creep behavior of cast Mg under stresses above the yield strength and the resultant texture evolution" *Can. Metallurgical Quart.*, 48(4) (2009) 419-432.
9. M. Fletcher et. al. "Evolution of strain and microstructure during creep of wrought AE42 and ZE10 magnesium alloys", *Trans. Of Indian Institute of Metals*, DOI: 10.1007/s12666-012-0200-3 (In press)
10. D. Sediako and S. Shook "Application of ND in in-situ studies of stress evolution in high temperature creep testing of magnesium alloys" *Magnesium Technology 2009*, TMS (2009) 255-259.